CEA–EDF–Inria Summer School — June 27 – July 1, 2022
Certification of errors in numerical simulations — EDF Lab, Paris-Saclay
https://ecoles-cea-edf-inria.fr/en/schools/ecole-analyse-numerique-2022/
Freefem++ web page: https://freefem.org/

Computer tutorial N°1

Certification of errors

Poisson equation, finite element method, flux reconstruction by averaging, flux reconstruction by equilibration, energy error, a posteriori error estimates, effectivity indices

Let $\Omega \subset \mathbb{R}^2$ be a polygon with Lipschitz boundary $\partial\Omega = \Gamma_{\rm D} \cup \Gamma_{\rm N}$. We consider the following model problem: for a given source term $f \in L^2(\Omega)$ and a given prescribed data $g_{\rm D}$ on the Dirichlet part of the boundary $\Gamma_{\rm D}$, find $u : \Omega \to \mathbb{R}$ such that

$$-\Delta u = f \qquad \text{in } \Omega, \tag{1a}$$
$$u = g_{\rm D} \qquad \text{on } \Gamma_{\rm D}, \tag{1b}$$
$$-\nabla u \cdot \boldsymbol{n}_\Omega = 0 \qquad \text{on } \Gamma_{\rm N}. \tag{1c}$$

The weak solution of problem (1) is a function $u \in H^1(\Omega)$ such that $u|_{\Gamma_{\rm D}} = g_{\rm D}$ and

$$(\nabla u, \nabla v) = (f, v) \qquad \forall v \in H^1_0(\Omega). \tag{2}$$

Let $\mathcal{T}_\ell$ be a triangulation of Ω. In this tutorial N°1, the mesh index ℓ is fixed, but in the forthcoming tutorials, we will consider sequence of meshes indexed by ℓ. The finite element method seeks for an approximate solution u_ℓ to the exact solution u in a finite-dimensional subspace V_ℓ^p of $H^1(\Omega)$. For a polynomial degree $p \geq 1$, we namely consider

$$V_\ell^p := \{v_\ell \in H^1(\Omega), v_\ell|_K \in \mathcal{P}_p(K) \quad \forall K \in \mathcal{T}_\ell\} = \mathcal{P}_p(\mathcal{T}_\ell) \cap H^1(\Omega). \tag{3}$$

Above, $\mathcal{P}_q(K)$ stands for the space of polynomials of total degree at most $q \geq 0$ on the mesh element $K \in \mathcal{T}_\ell$ and $\mathcal{P}_q(\mathcal{T}_\ell)$ denotes piecewise q-degree polynomials with respect to the mesh $\mathcal{T}_\ell$. Note that by the inclusion in $H^1(\Omega)$, the functions in V_ℓ^p have their traces continuous over all mesh faces. Then $u_\ell \in V_\ell^p$ needs to satisfy $u_\ell|_{\Gamma_{\rm D}} = g_{\rm D}$ and

$$(\nabla u_\ell, \nabla v_\ell) = (f, v_\ell) \qquad \forall v_\ell \in V_\ell^p \text{ such that } v_\ell|_{\Gamma_{\rm D}} = 0. \tag{4}$$

Exercices 1–6 below are designed for the case where Ω is a unit square, $\Gamma_{\rm D} = \partial\Omega$, $\Gamma_{\rm N} = \emptyset$, $g_{\rm D} = 0$, and $f = -2(x^2 + y^2) + 2(x + y)$. In this case, the exact solution is

$$u(x, y) = x(x - 1)y(y - 1), \tag{5}$$

which is smooth, $u \in C^\infty(\overline{\Omega})$. Exercice 7 then presents an extension to a singular case.

Exercice 1. (The finite element method)

1. Specify the user input in the Freefem++ script:

   ```
   int nds = 10; // number of mesh points on one domain unity edge
   ```

`macro Pcont P1` // Lagrange pw polynomial space of the FE approximation: "P1" or "P2" or "P3" or "P4"

`macro Pcontp P2` // polynomials for plotting the exact solution (ideally Pcont + 1): "P2" or "P3" or "P4"

`macro RTrec RT0` // Raviart–Thomas pw polynomial space for the averaged flux: "RT0" or "RT1" or "RT2"

`macro RT RT1` // Raviart–Thomas pw polynomial space for the equilibrated flux: "RT0" or "RT1" or "RT2"

`macro Pdisc P1dc` // Lagrange multipliers of the Raviart–Thomas space: "P0" or "P1dc" or "P2dc"

```
int verb = 0; // verbosity for demonstrations and debugging
```

```
bool RecFluxAver = 1, RecFlux = 1, Err = 1, Est = 1; // what to compute
```

```
bool PlotSolAppr = 1, PlotSolApprFluxes = 1, PlotRecFluxAver = 1,
PlotRecFlux = 1, PlotDetails = 1, PlotErr = 1, PlotEst = 1; // what to plot
```

2. Specify the exact solution u together with its derivatives, the right-hand side f, and the Dirichlet boundary datum g_{D}. This is done in the section `exact solution and its derivatives`.

3. Generate a triangular mesh $\mathcal{T}_\ell$ of Ω. In Freefem++, this is achieved via the command `mesh Th = square(nds,nds);`

4. Define the space V_ℓ^p from (3) in Freefem++: this is done via the command: `fespace Vh(Th,Pcont);`

5. Compute the finite element approximation u_ℓ given by (4). This is achieved via the commands

   ```
   Vh uh,vh; // FE approximation and test functions u_ℓ and v_ℓ
   ```

   ```
   varf a(uh,vh)=int2d(Th)(Grad(uh)'*Grad(vh))
    + int2d(Th)(f*vh) + on(1,2,3,4,uh=gd); // weak form
   ```

   ```
   matrix A=a(Vh,Vh,solver=SolverGlob); // construction of the stiffness matrix and choice of the solver
   ```

   ```
   real[int] b=a(0,Vh); // construction of the right-hand side vector
   ```

   ```
   uh[]=A^-1*b; // linear algebra solve
   ```

6. Plot the exact solution u and its finite element approximation u_ℓ. This is described in the Freefem++ script in the block `if(PlotSolAppr)`. Polynomial degrees $1 \le p \le 4$ in the definition of the finite element spaces (3) can be tested upon changing the parameter `Pcont` from `P1` to `P4` and `Pcontp` from `P2` to `P4`.

7. Plot the flux of the exact solution given by $-\nabla u$ and the flux of the finite element approximation given by $-\nabla u_\ell$. This is described in the Freefem++ script in the block `if(PlotSolApprFluxes)`. (In the FreeFem++ graphics window, the size of the arrows is modified by pressing "a" and "A".) Choose some two neighboring mesh elements and plot the details, as prepared in the script in the part with `if(PlotDetails)`. What do you observe? Does the exact flux $-\nabla u$ seem to be continuous across the mesh faces, or at least to have the normal component $-\nabla u \cdot \boldsymbol{n}_F$

continuous across any mesh face F? (Here, $\boldsymbol{n}_F$ is a unit normal vector of F.) Please notice that the latter, weaker, property, means that, for a given mesh face F, what "flows out" from one mesh element sharing F across F "flows in" the other mesh element sharing F. What about the flux approximation $-\nabla u_\ell$? Please inspect various polynomial degrees $1 \leq p \leq 4$.

Answer 1. (The finite element method)

The answers to items 1–5 are contained in the script `TP1.edp`. We now illustrate answers to questions 6–7. We take `nds=10`, so that there are $10 \times 10 \times 2$ isosceles triangles in the mesh $\mathcal{T}_\ell$.

6. One should obtain the results as in Figures 1 and 2.

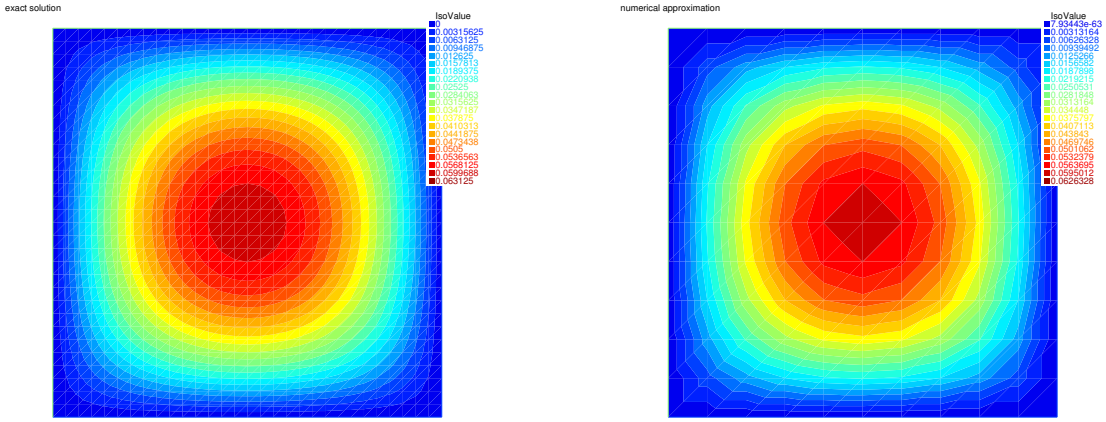

Figure 1: Exact solution u (left) and approximate solution u_ℓ (right, $p = 1$)

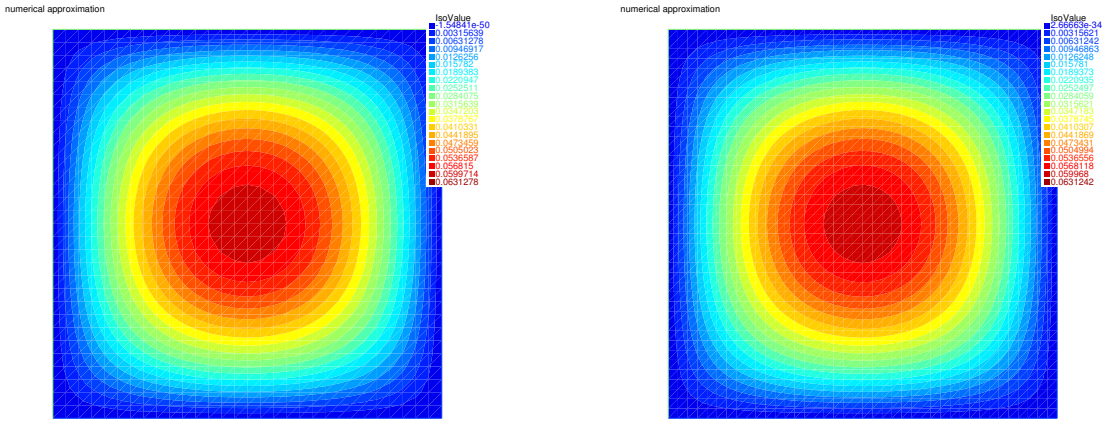

Figure 2: Approximate solution u_ℓ for $p = 2$ (left) and $p = 3$ (right)

7. One should obtain the results as in Figures 3 and 4. We plot the details of two mesh elements sharing the center vertex $(0.5, 0.5)$ in Figures 5 (exact flux $-\nabla u$) and 6 (approximate flux $-\nabla u_\ell$, $p = 1$). One in particular observes that the flux of the exact solution is a smooth, continuous vector field, so that it is continuous across the mesh faces. The flux of the finite element approximation, in turn, is a smooth vector field only inside each mesh element $K \in \mathcal{T}_\ell$. It is not continuous across the mesh faces, nor it has the normal component continuous across the mesh faces. This is clearly seen near the center and corners in Figure 3, right, and in Figure 6:

$-\nabla u_\ell$ for $p = 1$ is a piecewise constant, discontinuous, vector-valued field. This in particular means that, for a given mesh face F, it is not true that "flows out" from one mesh element sharing F across F "flows in" the other mesh element sharing F; the approximate flux $-\nabla u_\ell$ is unphysical, non-conservative. The exception is only the case $p = 4$: since the exact solution is here a polynomial of order 4, we actually in this case have $u_\ell(x, y) = u(x, y) = x(x - 1)y(y - 1)$.

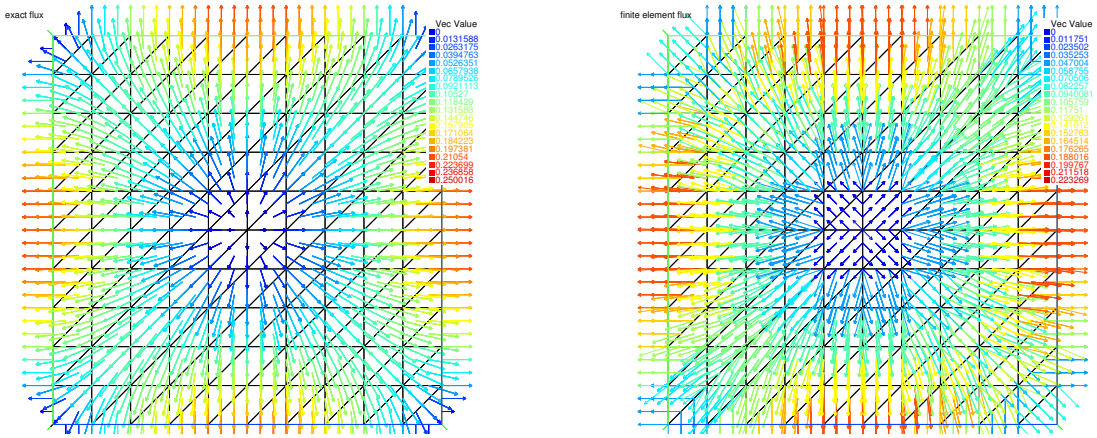

Figure 3: Flux of the exact solution $-\nabla u$ (left) and flux of the approximation $-\nabla u_\ell$ (right, $p = 1$)

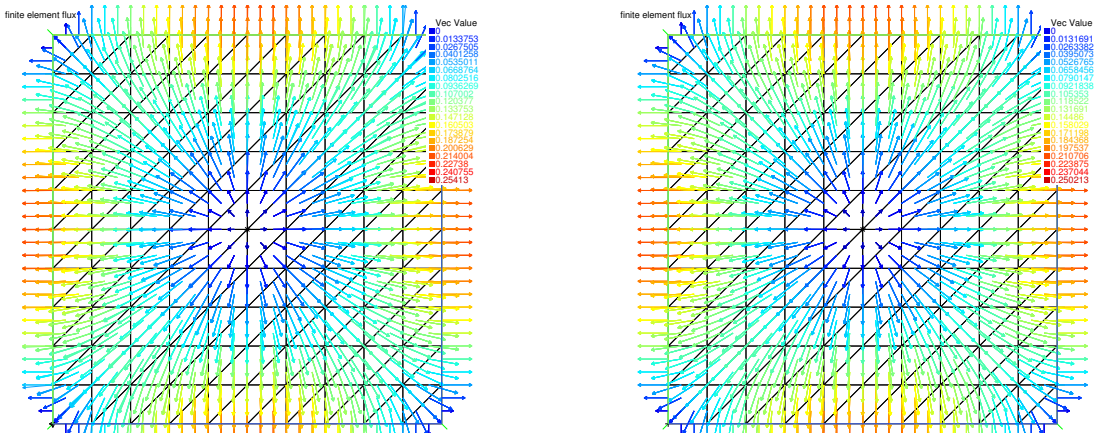

Figure 4: Flux of the approximation $-\nabla u_\ell$ for $p = 2$ (left) and $p = 3$ (right)

Exercice 2. (Flux reconstruction by averaging)

Let

$$\boldsymbol{V}_\ell^{p'} := \{\boldsymbol{v}_\ell \in \boldsymbol{H}(\mathrm{div}, \Omega), \boldsymbol{v}_\ell|_K \in \boldsymbol{\mathcal{RT}}_{p'}(K) \quad \forall K \in \mathcal{T}_\ell\} = \boldsymbol{\mathcal{RT}}_{p'}(\mathcal{T}_\ell) \cap \boldsymbol{H}(\mathrm{div}, \Omega) \tag{6}$$

be the Raviart–Thomas space of degree $p' \geq 0$. Here, $\boldsymbol{\mathcal{RT}}_{p'}(K) = [\mathcal{P}_{p'}(K)]^d + \boldsymbol{x}\mathcal{P}_{p'}(K)$ is the Raviart–Thomas space on a single mesh element $K \in \mathcal{T}_\ell$ and $\boldsymbol{\mathcal{RT}}_{p'}(\mathcal{T}_\ell)$ is the space of all functions that belong to $\boldsymbol{\mathcal{RT}}_{p'}(K)$ on each mesh element, the so-called broken Raviart–Thomas space. The inclusion into $\boldsymbol{H}(\mathrm{div}, \Omega)$ ensures that all functions from the space $\boldsymbol{V}_\ell^{p'}$ have their normal trace continuous over all mesh faces. We usually set the degree p' to p or to $p - 1$, i.e., equal to that of the finite element approximation u_ℓ ore one less.

1. Implement a flux reconstruction $\boldsymbol{\sigma}_\ell$ in the Raviart–Thomas space $\boldsymbol{V}_\ell^{p'}$ by averaging. This idea is to start from $-\nabla u_\ell$ and to use a simple averaging of the values that

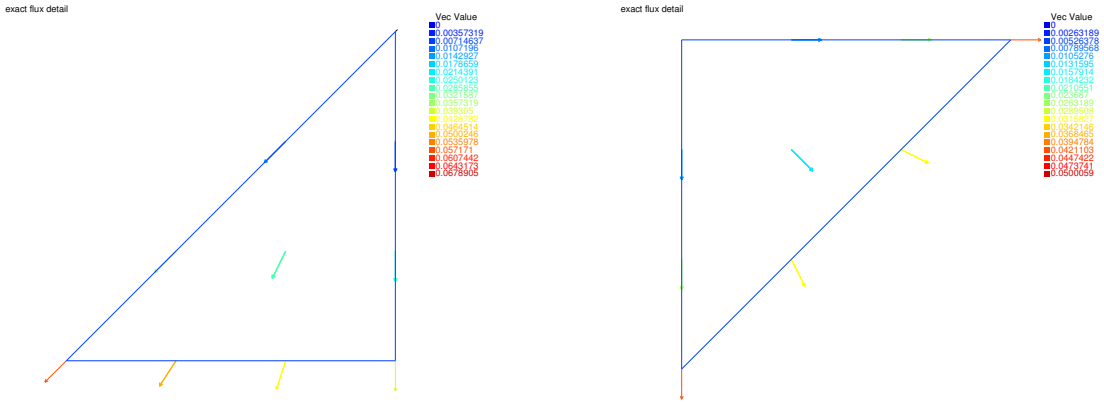

Figure 5: Flux of the exact solution $-\nabla u$, two neighboring elements sharing the center vertex $(0.5, 0.5)$

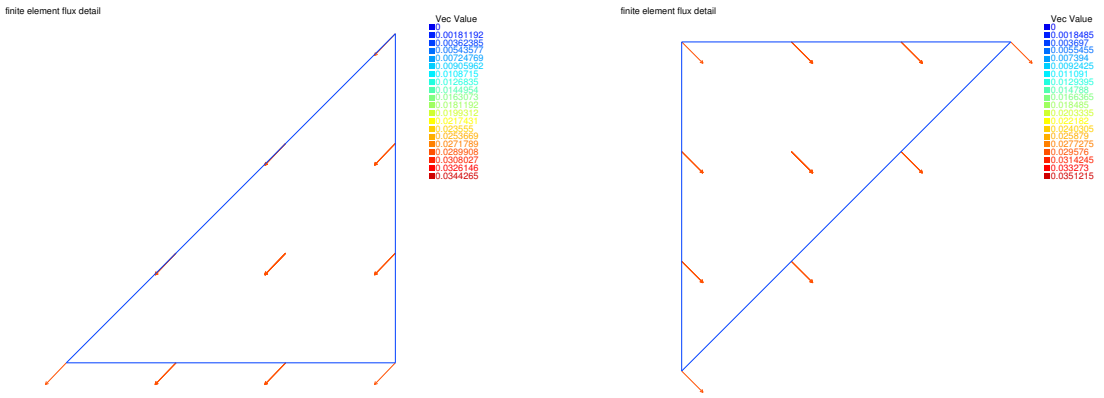

Figure 6: Flux of the approximation $-\nabla u_\ell$, $p = 1$, two neighboring elements sharing the center vertex $(0.5, 0.5)$

$-\nabla u_\ell$ takes in the degrees of freedom of Raviart–Thomas space $\boldsymbol{V}_\ell^{p'}$, i.e.,

$$\boldsymbol{\sigma}_\ell(DoF) := \text{ mean value of all } -\nabla u_\ell(DoF). \tag{7}$$

This is achieved by the FreeFem++ command `mean` in the section `if(RecFluxAver)`. The degree $p' = p - 1$ in (6) is in FreeFem++ script achieved by choosing the value of `RT` respectively as "RT0", "RT1", and "RT2" when `Pcont` is given by "P1", "P2", and "P3".

2. Plot the reconstructed flux $\boldsymbol{\sigma}_\ell$. What do you observe?

3. Plot the misfit of the optimal divergence of the reconstructed flux $\boldsymbol{\sigma}_\ell$. More precisely, the goal is to compute the following L^2 norms on each mesh element $K \in \mathcal{T}_\ell$:

$$\|\Pi_{p'} f - \nabla{\cdot}\boldsymbol{\sigma}_\ell\|_K, \tag{8}$$

where $\Pi_{p'}$ is the $L^2(\Omega)$-orthogonal projection onto discontinus piecewise polynomials of degree p' of the space $\mathcal{P}_{p'}(\mathcal{T}_\ell)$, i.e., $\Pi_{p'} f \in \mathcal{P}_{p'}(\mathcal{T}_\ell)$ is such that $(\Pi_{p'} f, v_\ell) = (f, v_\ell)$ for all $v_\ell \in \mathcal{P}_{p'}(\mathcal{T}_\ell)$, or, still equivalently, $(\Pi_{p'} f, v_\ell)_K = (f, v_\ell)_K$ for all $v_\ell \in \mathcal{P}_{p'}(K)$ and for all mesh elements $K \in \mathcal{T}_\ell$. For an equilibrated flux, the quantities in (8) would be zero. What do you observe here?

Answer 2. (Flux reconstruction by averaging)

The answer to item 1 is contained in the script in the section `if(RecFluxAver)`. We now illustrate answers to questions 2–3.

2. Figures 7 and 8 give the results. Details in the two mesh elements sharing the vertex $(0.5, 0.5)$ are depicted in Figure 9. It is now true that what "flows out" from one mesh element sharing a face F across F "flows in" the other mesh element sharing F, i.e., the normal component $\boldsymbol{\sigma}_\ell \cdot \boldsymbol{n}_F$ is continuous across any mesh face F (though the tangential component of $\boldsymbol{\sigma}_\ell$, and thus $\boldsymbol{\sigma}_\ell$, may be discontinuous). In that sense, and in contrast to $-\nabla u_\ell$, the flux $\boldsymbol{\sigma}_\ell$ is now physical, mass conservative.

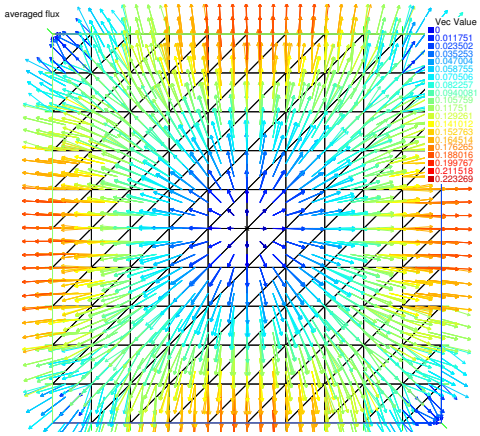

Figure 7: Averaged flux $\boldsymbol{\sigma}_\ell$ for $p = 1$ and $p' = 0$

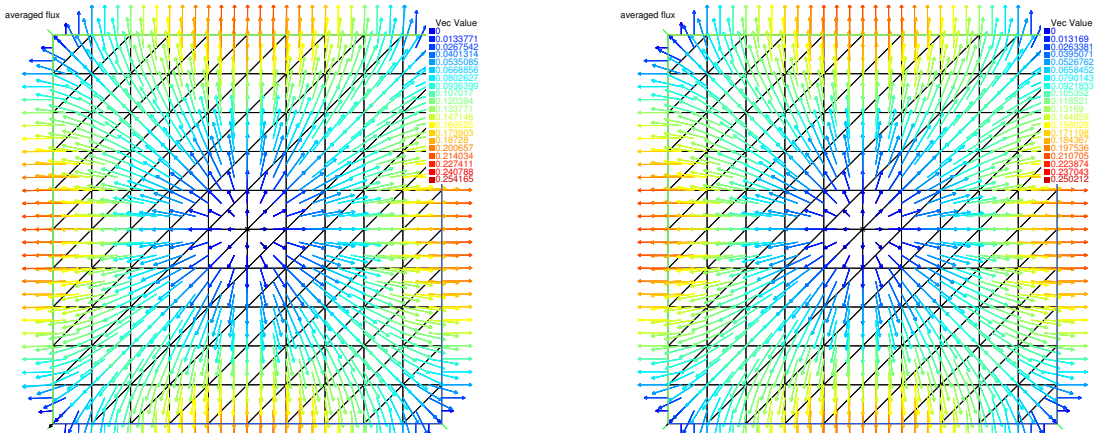

Figure 8: Averaged flux $\boldsymbol{\sigma}_\ell$ for $p = 2$ and $p' = 1$ (left) and $p = 3$ and $p' = 2$ (right)

3. Figures 10 and 11 present the results. They unfortunately reveal that the fluxes reconstructed by the simple (and fast) averaging (7) are still unphysical, non mass conservative, as they do not satisfy the equilibrium with the source term $\nabla \cdot \boldsymbol{\sigma}_\ell = \Pi_{p'} f$ (neglecting the difference $f - \Pi_{p'} f$), neither the weaker condition

$$(\nabla \cdot \boldsymbol{\sigma}_\ell, 1)_K = (f, 1)_K \qquad \forall K \in \mathcal{T}_\ell. \tag{9}$$

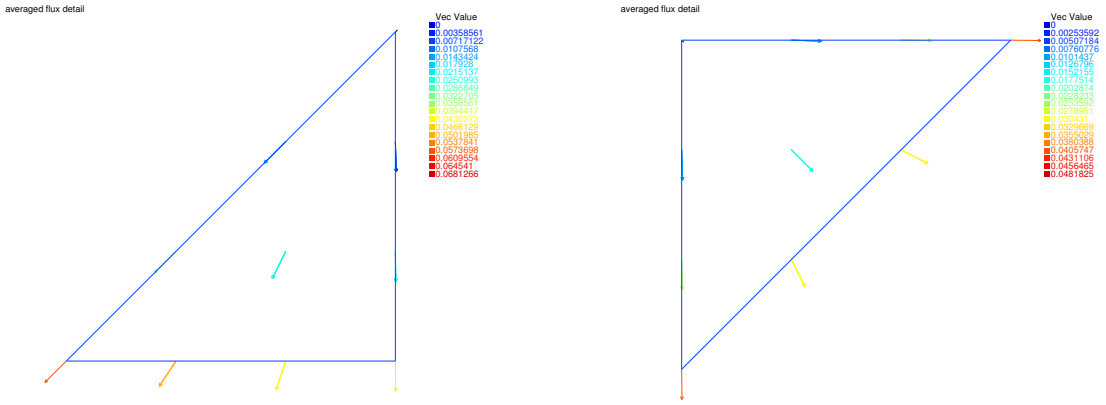

Figure 9: Averaged flux $\boldsymbol{\sigma}_\ell$, $p = 1$ and $p' = 0$, two neighboring elements sharing the center vertex $(0.5, 0.5)$

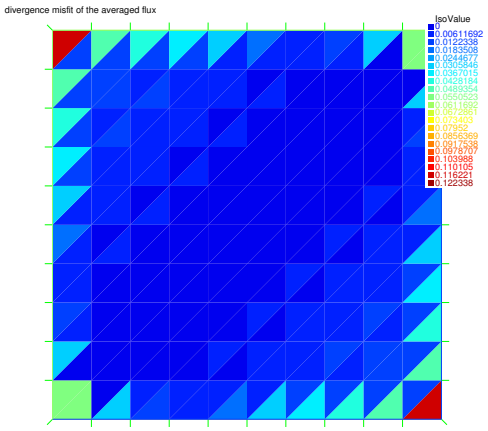

Figure 10: Divergence misfit of the averaged flux $\boldsymbol{\sigma}_\ell$, $p = 1$ and $p' = 0$

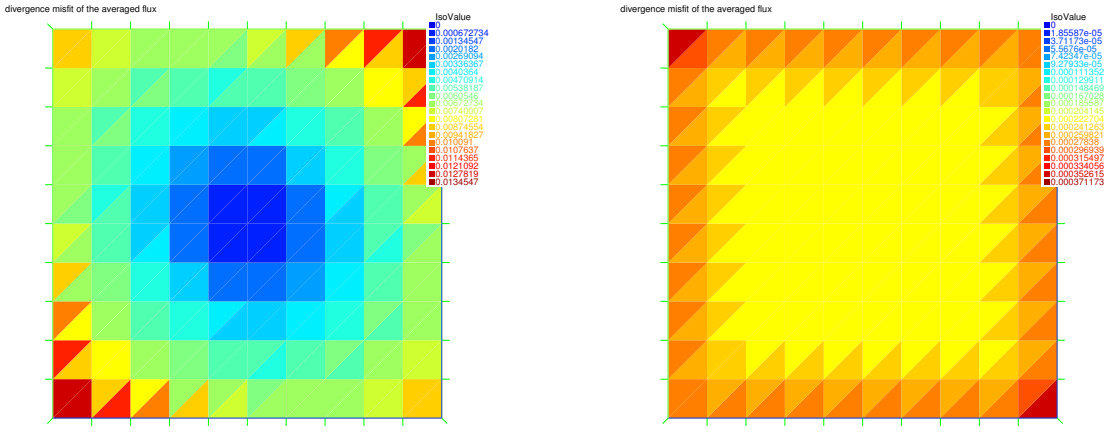

Figure 11: Divergence misfit of the averaged flux $\boldsymbol{\sigma}_\ell$, $p = 2$ and $p' = 1$ (left) and $p = 3$ and $p' = 2$ (right)

Exercice 3. (Flux reconstruction by equilibration)

Let the Raviart–Thomas space of degree $p' \geq 0$ be given by (6).

1. Implement the equilibrated flux reconstruction $\boldsymbol{\sigma}_\ell$ in the Raviart–Thomas space $\boldsymbol{V}_\ell^{p'}$. Let $-\nabla u_\ell$ be computed. For each fixed mesh vertex $\boldsymbol{a} \in \mathcal{V}_\ell$, let $\mathcal{T}_{\boldsymbol{a}}$ be the patch of all mesh elements from $\mathcal{T}_\ell$ that share the vertex $\boldsymbol{a}$ and $\omega_{\boldsymbol{a}}$ the corresponding patch subdomain. Let $\psi^{\boldsymbol{a}}$ be the hat function, i.e., the unique continuous and piecewise 1-st order polynomial that takes the value 1 in the vertex $\boldsymbol{a}$ and the value 0 in all other mesh vertices; note that the support of $\psi^{\boldsymbol{a}}$ is the patch subdomain $\omega_{\boldsymbol{a}}$. For a vertex $\boldsymbol{a}$ inside the computational domain Ω, let $\boldsymbol{H}_0(\mathrm{div}, \omega_{\boldsymbol{a}})$ be the subspace of all functions from $\boldsymbol{H}(\mathrm{div}, \omega_{\boldsymbol{a}})$ whose normal trace vanishes on $\partial\omega_{\boldsymbol{a}}$. For a vertex $\boldsymbol{a}$ on the boundary of Ω, we only request the normal trace to vanish on 1) the part of $\partial\omega_{\boldsymbol{a}}$ where $\psi^{\boldsymbol{a}}$ is zero (typically the part of $\partial\omega_{\boldsymbol{a}}$ not contained in $\partial\Omega$); and 2) $\Gamma_{\mathrm{N}} \cap \partial\omega_{\boldsymbol{a}}$.

   The local equilibration has two stages: first we need to solve the local quadratic minimization problem

$$\boldsymbol{\sigma}_\ell^{\boldsymbol{a}} := \arg \min_{\substack{\boldsymbol{v}_\ell \in \boldsymbol{\mathcal{RT}}_{p'}(\mathcal{T}_{\boldsymbol{a}}) \cap \boldsymbol{H}_0(\mathrm{div}, \omega_{\boldsymbol{a}}) \\ \nabla\cdot\boldsymbol{v}_\ell = \Pi_{p'}(f\psi^{\boldsymbol{a}} - \nabla u_\ell \cdot \nabla\psi^{\boldsymbol{a}})}} \|\psi^{\boldsymbol{a}} \nabla u_\ell + \boldsymbol{v}_\ell\|_{\omega_{\boldsymbol{a}}}^2 \tag{10a}$$

   for all $\boldsymbol{a} \in \mathcal{V}_\ell$. Then we run over all mesh vertices $\boldsymbol{a} \in \mathcal{V}_\ell$ and sum the individual contributions $\boldsymbol{\sigma}_\ell^{\boldsymbol{a}}$ as

$$\boldsymbol{\sigma}_\ell := \sum_{\boldsymbol{a} \in \mathcal{V}_\ell} \boldsymbol{\sigma}_\ell^{\boldsymbol{a}}. \tag{10b}$$

   Evoking the Euler–Lagrange optimality conditions of (10a), (10a) can be equivalently written as: find $\boldsymbol{\sigma}_\ell^{\boldsymbol{a}} \in \boldsymbol{\mathcal{RT}}_{p'}(\mathcal{T}_{\boldsymbol{a}}) \cap \boldsymbol{H}_0(\mathrm{div}, \omega_{\boldsymbol{a}})$ with $\nabla\cdot\boldsymbol{\sigma}_\ell^{\boldsymbol{a}} = \Pi_{p'}(f\psi^{\boldsymbol{a}} - \nabla u_\ell \cdot \nabla\psi^{\boldsymbol{a}})$ such that

$$(\boldsymbol{\sigma}_\ell^{\boldsymbol{a}}, \boldsymbol{v}_\ell)_{\omega_{\boldsymbol{a}}} = -(\psi^{\boldsymbol{a}} \nabla u_\ell, \boldsymbol{v}_\ell)_{\omega_{\boldsymbol{a}}} \qquad \forall \boldsymbol{v}_\ell \in \boldsymbol{\mathcal{RT}}_{p'}(\mathcal{T}_{\boldsymbol{a}}) \cap \boldsymbol{H}_0(\mathrm{div}, \omega_{\boldsymbol{a}}) \text{ with } \nabla\cdot\boldsymbol{v}_\ell = 0. \tag{11}$$

   One could now implement (11), but one would need for this purpose to construct a basis of the Raviart–Thomas space of piecewise polynomial vector-valued fields from $\boldsymbol{\mathcal{RT}}_{p'}(\mathcal{T}_{\boldsymbol{a}}) \cap \boldsymbol{H}_0(\mathrm{div}, \omega_{\boldsymbol{a}})$ with the property $\nabla\cdot\boldsymbol{v}_\ell = 0$. To avoid this, we further rewrite equivalently (11) as: find $\boldsymbol{\sigma}_\ell^{\boldsymbol{a}} \in \boldsymbol{\mathcal{RT}}_{p'}(\mathcal{T}_{\boldsymbol{a}}) \cap \boldsymbol{H}_0(\mathrm{div}, \omega_{\boldsymbol{a}})$, together with the additional scalar-valued piecewise polynomial $\gamma_\ell^{\boldsymbol{a}} \in \mathcal{P}_{p'}(\mathcal{T}_{\boldsymbol{a}})$, such that

$$(\boldsymbol{\sigma}_\ell^{\boldsymbol{a}}, \boldsymbol{v}_\ell)_{\omega_{\boldsymbol{a}}} - (\gamma_\ell^{\boldsymbol{a}}, \nabla\cdot\boldsymbol{v}_\ell)_{\omega_{\boldsymbol{a}}} = -(\psi^{\boldsymbol{a}} \nabla u_\ell, \boldsymbol{v}_\ell)_{\omega_{\boldsymbol{a}}} \qquad \forall \boldsymbol{v}_\ell \in \boldsymbol{\mathcal{RT}}_{p'}(\mathcal{T}_{\boldsymbol{a}}) \cap \boldsymbol{H}_0(\mathrm{div}, \omega_{\boldsymbol{a}}), \tag{12a}$$

$$(\nabla\cdot\boldsymbol{\sigma}_\ell^{\boldsymbol{a}}, q_\ell)_{\omega_{\boldsymbol{a}}} = (f\psi^{\boldsymbol{a}} - \nabla u_\ell \cdot \nabla\psi^{\boldsymbol{a}}, q_\ell)_{\omega_{\boldsymbol{a}}} \quad \forall q_\ell \in \mathcal{P}_{p'}(\mathcal{T}_{\boldsymbol{a}}). \tag{12b}$$

2. Plot the finite element flux $-\nabla u_\ell$, the hat-function-weighted finite element flux $-\psi^{\boldsymbol{a}} \nabla u_\ell$, the equilibrated flux contribution $\boldsymbol{\sigma}_\ell^{\boldsymbol{a}}$, and the hat-function-weighted exact flux $-\psi^{\boldsymbol{a}} \nabla u$ on each patch subdomain $\omega_{\boldsymbol{a}}$. Describe what you observe: differences and similarities between the plots, sizes of these vector fields close to the vertex $\boldsymbol{a}$ and close to the boundary of the patch subdomain $\omega_{\boldsymbol{a}}$ (not shared by the boundary $\partial\Omega$), continuity across the mesh faces, and normal component continuity across the mesh faces. (Attention, FreeFem++ mainly distinguishes the sizes of vector fields by color and not by size.)

3. Plot the reconstructed flux $\boldsymbol{\sigma}_\ell$. What do you observe?

4. Plot the divergence misfit of the reconstructed flux $\boldsymbol{\sigma}_\ell$. More precisely, the idea is to compute the elementwise L^2 norms (8). From definition (10), these should be zero. What do you observe here?

Answer 3. (Flux reconstruction by equilibration)

The answer to item 1 is contained in the script `TP1.edp` in the function `ComputEquilFlux()`. We now illustrate the answers to questions 2–4.

2. Figure 12 collects the results. We have chosen there the middle patch around the center vertex $\boldsymbol{a} = (0.5, 0.5)$. For $p = 1$, the finite element flux $-\nabla u_\ell$ is piecewise constant and discontinuous from one mesh element to the other. The hat-function-weighted finite element flux $-\psi^{\boldsymbol{a}}\nabla u_\ell$ scales the finite element flux $-\nabla u_\ell$ such that its values close to the vertex $\boldsymbol{a} = (0.5, 0.5)$ are similar to those of $-\nabla u_\ell$, but its values close to the patch subdomain boundary $\partial\omega_{\boldsymbol{a}}$ vanish; we call it cut-off by the hat function $\psi^{\boldsymbol{a}}$. Remark that $-\psi^{\boldsymbol{a}}\nabla u_\ell$ is still discontinuous from one mesh element to the other. From the minimization form (10a), the equilibrated flux contribution $\boldsymbol{\sigma}_\ell^{\boldsymbol{a}}$ tries to stay as close as possible to $-\psi^{\boldsymbol{a}}\nabla u_\ell$, but as the same time has to ensure that its normal trace $\boldsymbol{\sigma}_\ell^{\boldsymbol{a}}\cdot\boldsymbol{n}_F$ is continuous across all the faces F sharing the vertex $\boldsymbol{a}$ and vanishes at the patch subdomain boundary $\partial\omega_{\boldsymbol{a}}$. Moreover, the divergence constraint $\nabla\cdot\boldsymbol{\sigma}_\ell^{\boldsymbol{a}} = \Pi_{p'}(f\psi^{\boldsymbol{a}} - \nabla u_\ell\cdot\nabla\psi^{\boldsymbol{a}})$ has to be ensured.

   There are two sets of arrows on the horizontal middle line $y = 0.5$, since one is plotted from the triangles below the line $y = 0.5$, and the other from above $y = 0.5$. Interestingly enough, they do not always coincide, so that the flux $\boldsymbol{\sigma}_\ell^{\boldsymbol{a}}$ itself is not continuous (a similar observation also holds for the vertical line $x = 0.5$). Importantly, though, their y-components, representing $\boldsymbol{\sigma}_\ell^{\boldsymbol{a}}\cdot\boldsymbol{n}$ across the line $y = 0.5$, with $\boldsymbol{n} = (0, 1)^{\mathrm{t}}$, are of the same sign and magnitude, so that the normal trace $\boldsymbol{\sigma}_\ell^{\boldsymbol{a}}\cdot\boldsymbol{n}$ of $\boldsymbol{\sigma}_\ell^{\boldsymbol{a}}$ is indeed continuous across all mesh faces sharing the vertex $\boldsymbol{a}$. Ideally, $\boldsymbol{\sigma}_\ell^{\boldsymbol{a}}$ should approach the hat-function-weighted exact flux $-\psi^{\boldsymbol{a}}\nabla u$, which happens here to be fully continuous and not just normal-trace continuous.

3. Figures 13 and 14 give the results. Details in the two mesh elements close to the center vertex $(0.5, 0.5)$ are depicted in Figure 15. As above for flux reconstruction by averaging, it is also true here that what "flows out" from one mesh element sharing F across F "flows in" the other mesh element sharing F. Thus, in this sense, in contrast to $-\nabla u_\ell$, the flux $\boldsymbol{\sigma}_\ell$ is physical, mass conservative.

4. Figures 16 and 17 present the results. They confirm that the fluxes reconstructed by the local equilibration (10) are now fully physical, mass conservative, as they satisfy the equilibrium with the source term

$$\nabla\cdot\boldsymbol{\sigma}_\ell = \Pi_{p'} f$$

   (neglecting the difference $f - \Pi_{p'} f$), as well as, of course, the weaker condition (9). Please note that the fact that al the values in Figures 16 and 17 are not exactly equal to 0 is only because of rounding errors.

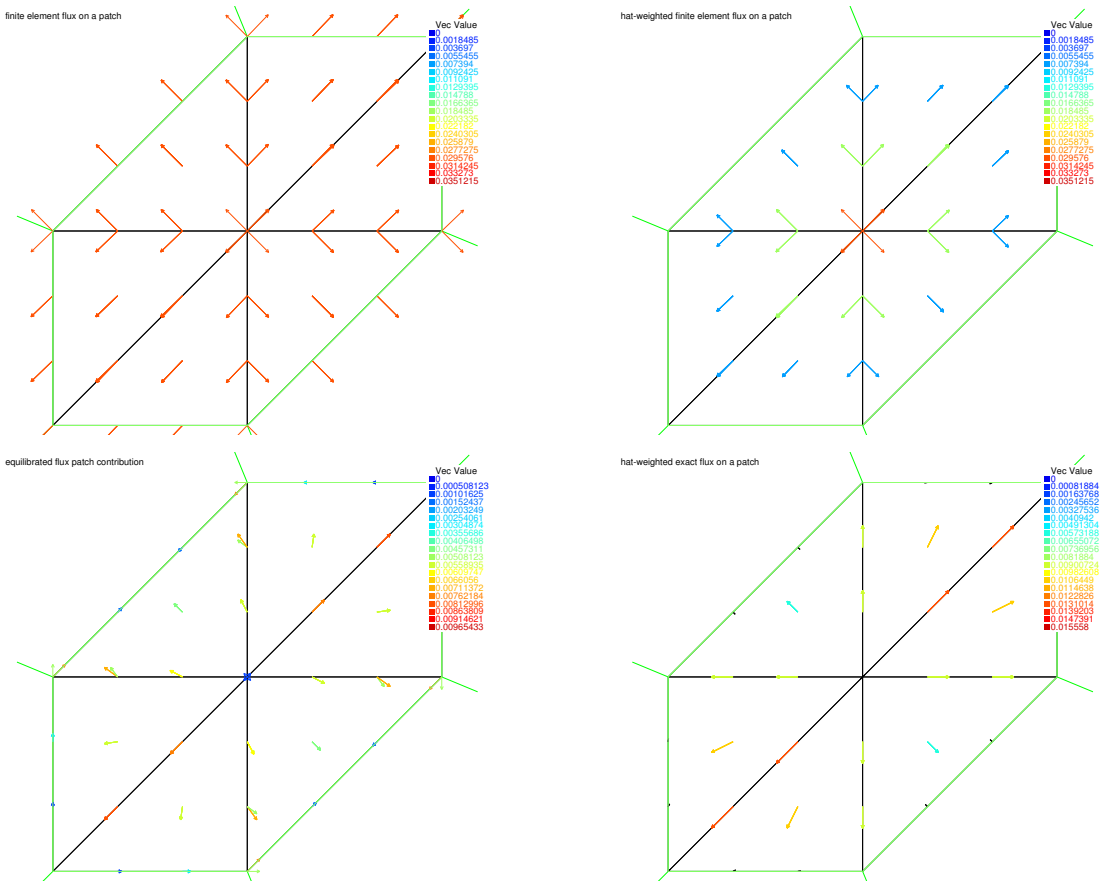

Figure 12: Finite element flux $-\nabla u_\ell$ (top left), the hat-function-weighted finite element flux $-\psi^{\boldsymbol{a}}\nabla u_\ell$ (top right), the equilibrated flux contribution $\boldsymbol{\sigma}_\ell^{\boldsymbol{a}}$ (bottom left), and the hat-function-weighted exact flux $-\psi^{\boldsymbol{a}}\nabla u$ (bottom right) on a patch subdomain $\omega_{\boldsymbol{a}}$ around the center vertex $\boldsymbol{a} = (0.5, 0.5)$, $p = 1$ and $p' = 1$

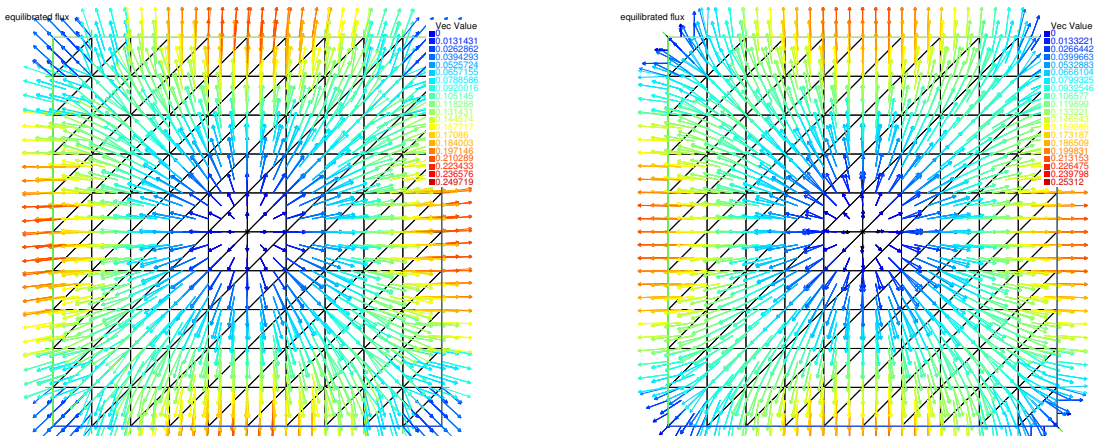

Figure 13: Equilibrated flux $\boldsymbol{\sigma}_\ell$, $p = 1$ and $p' = 0$ (left) and $p = 1$ and $p' = 1$ (right)

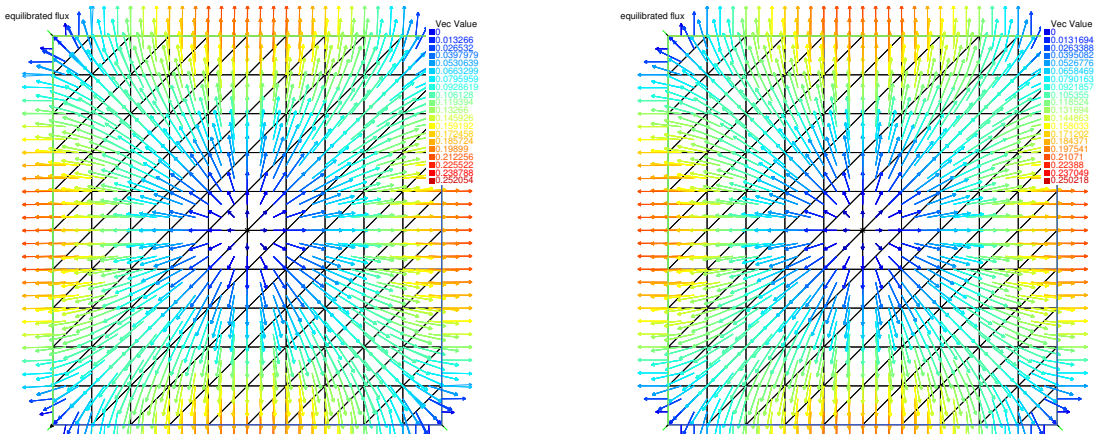

Figure 14: Equilibrated flux $\boldsymbol{\sigma}_\ell$, $p = 2$ and $p' = 1$ (left) and $p = 3$ and $p' = 2$ (right)

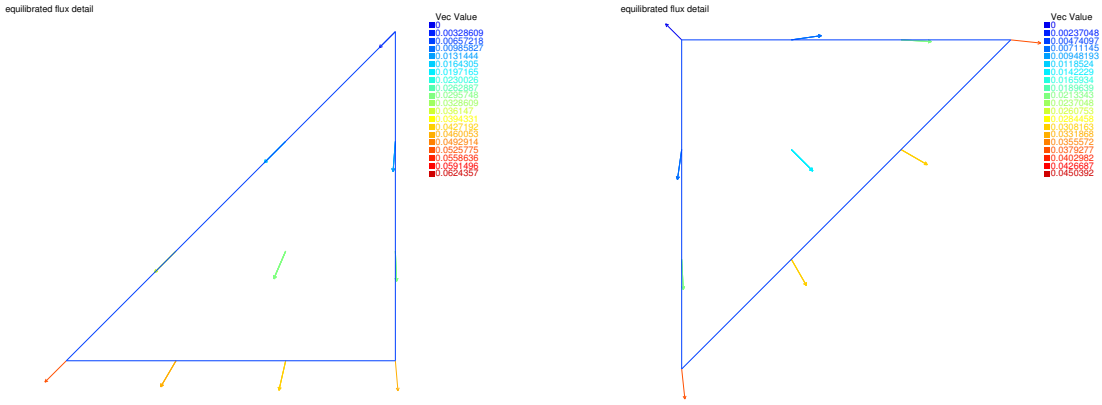

Figure 15: Equilibrated flux $\boldsymbol{\sigma}_\ell$, $p = 1$ and $p' = 1$, two neighboring elements sharing the center vertex $(0.5, 0.5)$

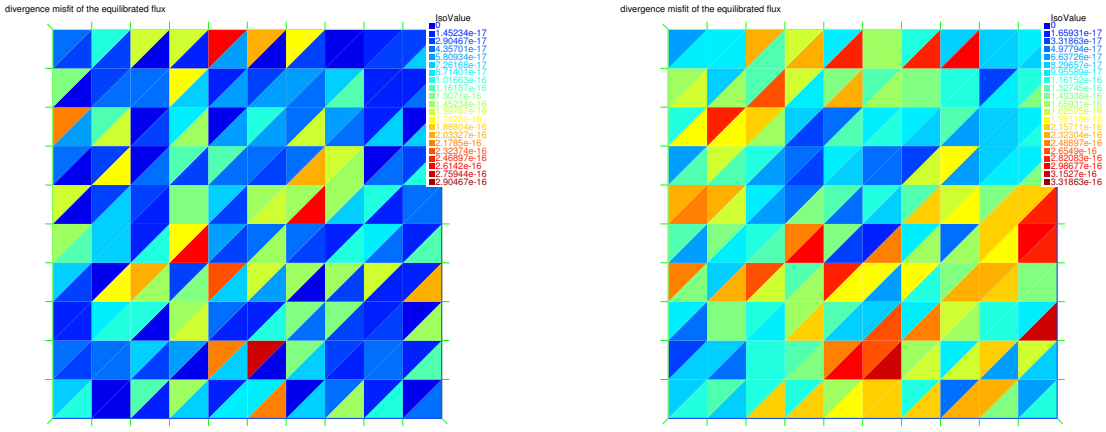

Figure 16: Divergence misfit of the equilibrated flux $\boldsymbol{\sigma}_\ell$, $p = 1$ and $p' = 0$ (left) and $p = 1$ and $p' = 1$ (right)

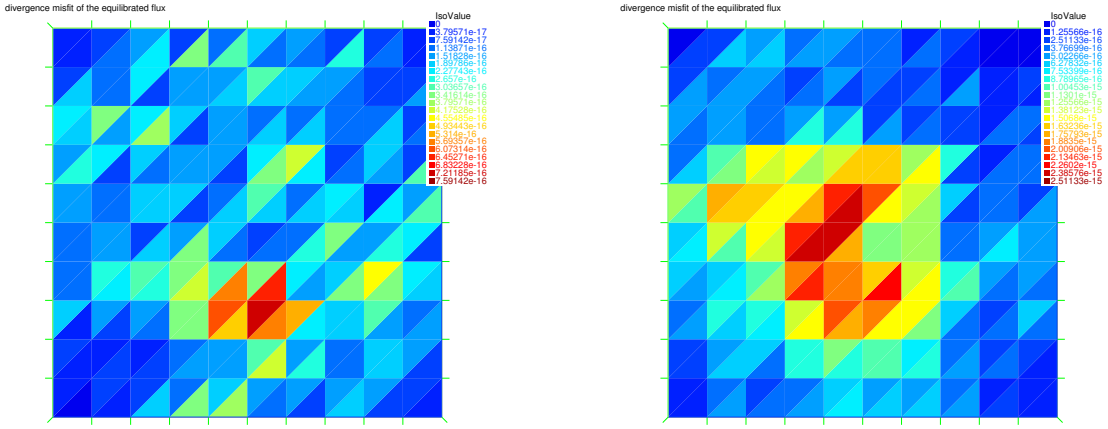

Figure 17: Divergence misfit of the equilibrated flux $\boldsymbol{\sigma}_\ell$, $p = 2$ and $p' = 1$ (left) and $p = 3$ and $p' = 2$ (right)

Exercice 4. (Error)

We will compute here the errors between the exact solution u of (2) and its finite element approximation u_ℓ of (4).

1. Compute the error $\|\nabla(u - u_\ell)\|$, as well as its elementwise contributions

$$\|\nabla(u - u_\ell)\|_K \tag{13}$$

   for each mesh element $K \in \mathcal{T}_\ell$.

2. Plot the elementwise error contributions (13).

Answer 4. (Error)

The answers to this part are contained in the FreeFem++ function `ErrDist()`.

1. This is achieved via the FreeFem++ function `int2d(Th)`.

2. The error distributions are depicted in Figures 18–19 below, alongside with the corresponding estimators by equilibrated fluxes.

Exercice 5. (A posteriori error estimators by equilibrated fluxes)

We will now compute the a posteriori error estimators on the error between the exact solution u of (2) and its finite element approximation u_ℓ of (4). We start by the equilibrated fluxes of Exercice 3, in the setting with $p' = p$ according to the theory developed in the lectures. Recall that in this case, we have

$$\|\nabla(u - u_\ell)\| \leq \eta_\ell := \left\{ \sum_{K \in \mathcal{T}_\ell} \left[\|\nabla u_\ell + \boldsymbol{\sigma}_\ell\|_K + \frac{h_K}{\pi} \|f - \Pi_{p'} f\|_K \right]^2 \right\}^{\frac{1}{2}}. \tag{14}$$

1. Plot the elementwise a posteriori error estimators $\left[\|\nabla u_\ell + \boldsymbol{\sigma}_\ell\|_K + \frac{h_K}{\pi} \|f - \Pi_{p'} f\|_K \right]$. Compare them to the plots of the elementwise errors from Exercice 4. What do you observe?

2. Plot the "data oscillation" part of the estimators given by $\frac{h_K}{\pi} \|f - \Pi_{p'} f\|_K$.

3. Compare the size of the a posteriori error estimator η_ℓ to the size of the error $\|\nabla(u - u_\ell)\|$. This is best done in terms of the so-called effectivity index

$$I_{\text{eff},\ell} := \frac{\eta_\ell}{\|\nabla(u - u_\ell)\|}. \tag{15}$$

   What do you observe?

Answer 5. (A posteriori error estimators by equilibrated fluxes)

1. The answer is given in Figures 18–19. We observe an almost perfect match between the actual and estimated elementwise error distributions.

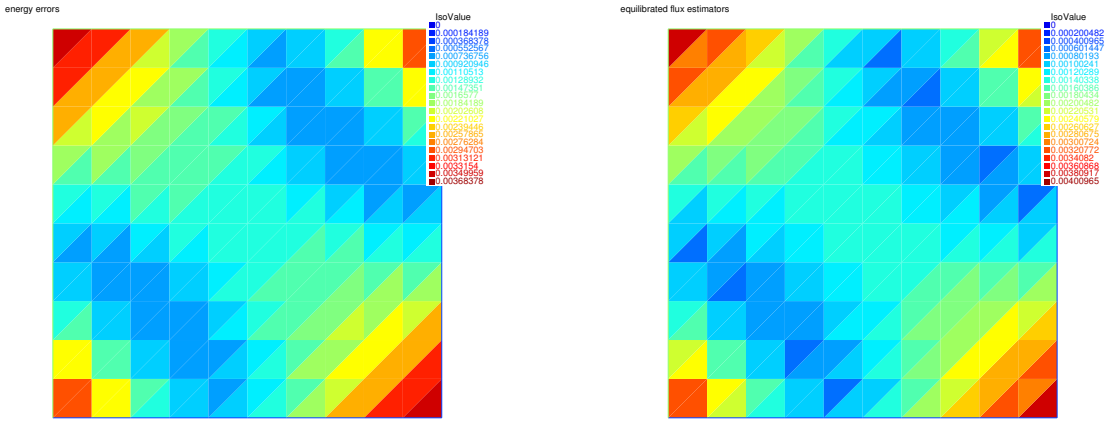

Figure 18: Elementwise errors $\|\nabla(u-u_\ell)\|_K$ (left) and estimators $\left[\|\nabla u_\ell+\boldsymbol{\sigma}_\ell\|_K+\frac{h_K}{\pi}\|f-\Pi_{p'}f\|_K\right]$ (right), equilibrated fluxes, $p=1$ and $p'=1$

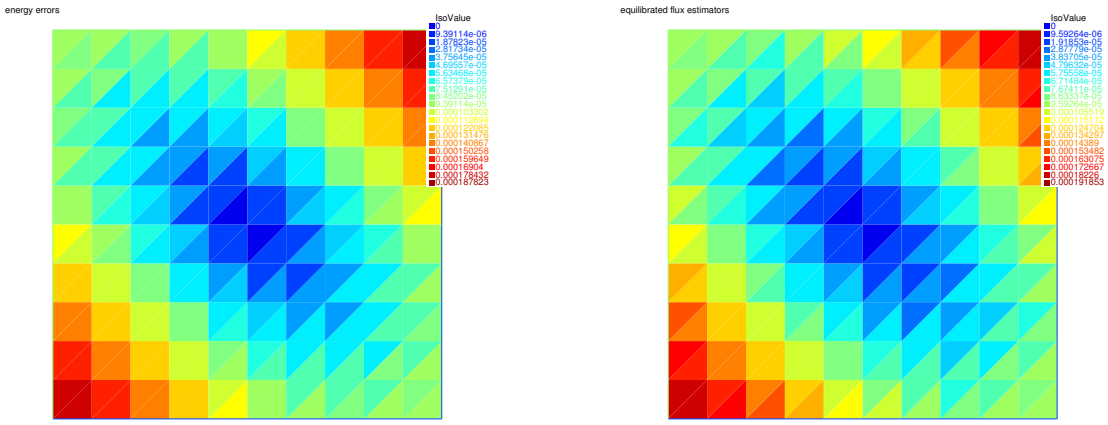

Figure 19: Elementwise errors $\|\nabla(u-u_\ell)\|_K$ (left) and estimators $\left[\|\nabla u_\ell+\boldsymbol{\sigma}_\ell\|_K+\frac{h_K}{\pi}\|f-\Pi_{p'}f\|_K\right]$ (right), equilibrated fluxes, $p=2$ and $p'=2$

2. The answer is plotted in Figure 20. The elementwise data oscillations $\frac{h_K}{\pi}\|f-\Pi_{p'}f\|_K$ take much smaller values than the elementwise errors $\|\nabla(u-u_\ell)\|_K$ (they converge two orders of magnitude faster than the error in the mesh-size h for elementwise smooth f). Moreover, for $p'=2$, where $\Pi_{p'}f=f$, we only observe rounding errors.

3. The effectivity indices $I_{\text{eff},\ell}$ given by (17) are greater or equal to one and tend to one with both the mesh refinement and polynomial degree increase. For Figures 18–19, they respectively take the values 1.04445 and 1.01167.

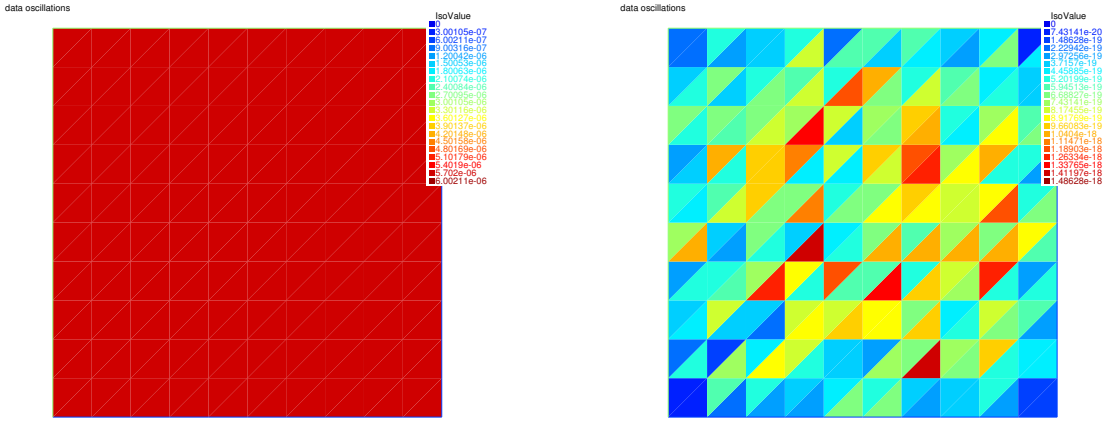

Figure 20: Elementwise data oscillations $\frac{h_K}{\pi}\|f - \Pi_{p'} f\|_K$ for $p = 1$ and $p' = 1$ (left) and $p = 2$ and $p' = 2$ (right)

Exercice 6. (A posteriori error estimators by averaged fluxes)

We will now also compute the a posteriori error estimators for the averaged fluxes of Exercice 2. In this case, there is no guaranteed upper bound, though we may still hope to obtain

$$\|\nabla(u - u_\ell)\| \lesssim \|\nabla u_\ell + \boldsymbol{\sigma}_\ell\|. \tag{16}$$

1. Plot the elementwise a posteriori error estimators $\|\nabla u_\ell + \boldsymbol{\sigma}_\ell\|_K$. Compare them to the plots of the elementwise errors from Exercice 4. What do you observe?

2. Compare the size of the a posteriori error estimator $\|\nabla u_\ell + \boldsymbol{\sigma}_\ell\|$ to the size of the error $\|\nabla(u - u_\ell)\|$. This is best done in terms of the so-called effectivity index

$$I_{\mathrm{eff},\ell} := \frac{\|\nabla u_\ell + \boldsymbol{\sigma}_\ell\|}{\|\nabla(u - u_\ell)\|}. \tag{17}$$

   What do you observe?

Answer 6. (A posteriori error estimators by averaged fluxes)

1. The answer is given in Figures 21–22. We observe a reasonable match, though weaker than in Figures 18–19.

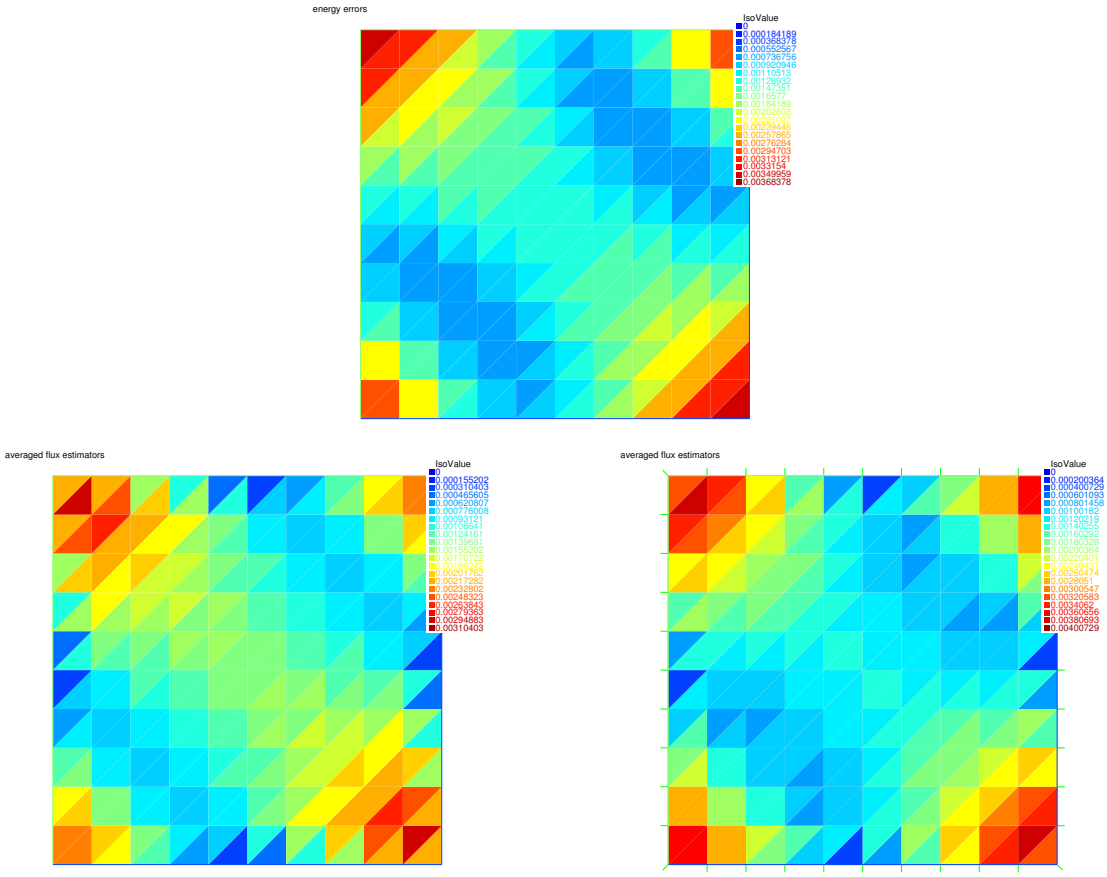

Figure 21: Elementwise errors $\|\nabla(u - u_\ell)\|_K$ (top) and estimators $\|\nabla u_\ell + \boldsymbol{\sigma}_\ell\|_K$ (bottom), averaged fluxes; $p = 1$ and $p' = 1$ (left) and $p = 1$ and $p' = 0$ (right)

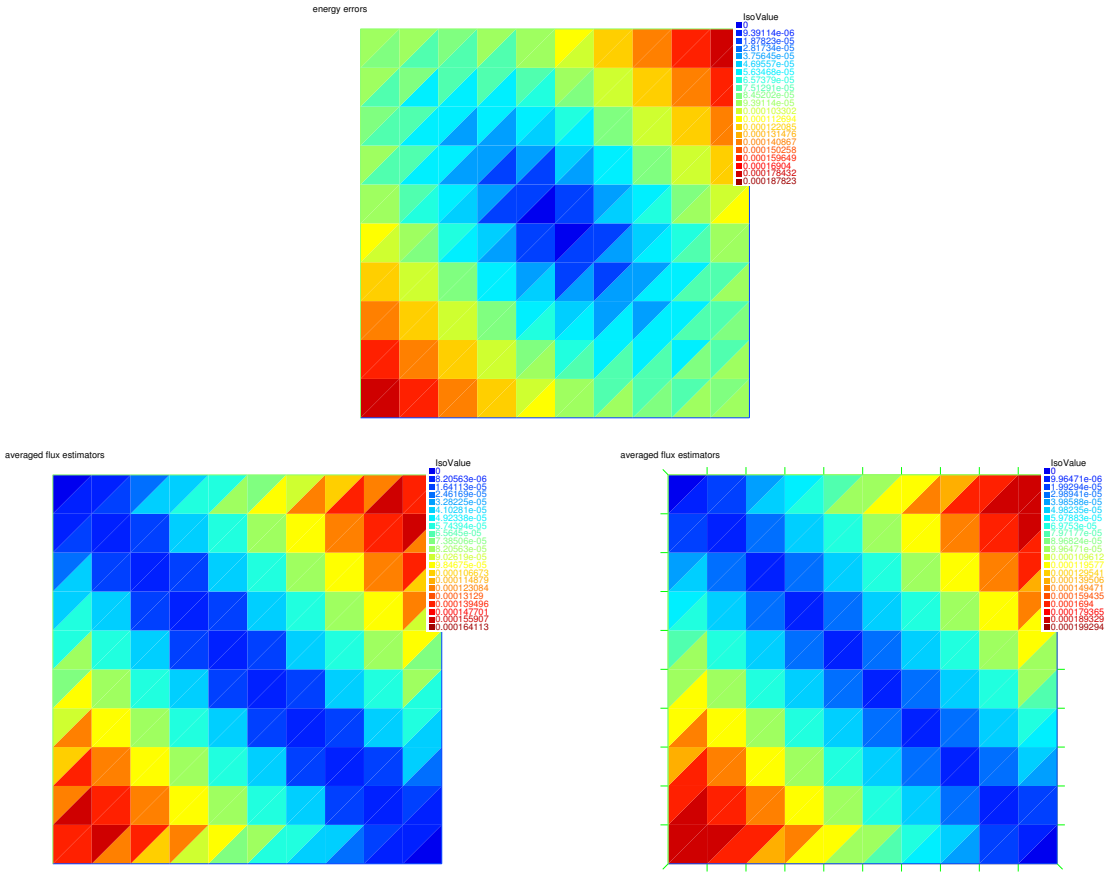

Figure 22: Elementwise errors $\|\nabla(u-u_\ell)\|_K$ (top) and estimators $\|\nabla u_\ell + \boldsymbol{\sigma}_\ell\|_K$ (bottom), averaged fluxes; $p=2$ and $p'=2$ (left) and $p=2$ and $p'=1$ (right)

2. The effectivity indices $I_{\mathrm{eff},\ell}$ given by (17) are not necessarily greater or equal to one here, and they do not necessarily tend to one with mesh refinement or polynomial degree increase. For Figures 21–22, they take the values 0.908161 ($p'=1$) and 1.12652 ($p'=0$), respectively 0.811856 ($p'=2$) and 1.01725 ($p'=1$).

Exercice 7. (L-shaped domain with a singular solution)

The goal here is to extend all the previous exercices to the L-shaped domain $\Omega = (-1,1)\times(-1,1)\setminus[0,1]\times[-1,0]$ together with the exact solution written, in polar coordinates, as

$$u(r,\theta) = r^{\frac{2}{3}}\sin(2\theta/3). \tag{18}$$

We remark that we consider here $\theta \in (0, 3\pi/2)$. The corresponding source term $f = 0$, and we take $g_{\mathrm{D}} = u$ on $\Gamma_{\mathrm{D}} = \partial\Omega$ and $\Gamma_{\mathrm{N}} = \emptyset$. The point is that whereas u given by (5) is smooth, u given by (18) is singular, $u \in H^{1+\frac{2}{3}-\varepsilon}(\Omega)$ for any $\varepsilon > 0$ only, with the gradient exploding at the re-entrant corner $(0,0)$.

Answer 7. (L-shaped domain with a singular solution)

Figures 23–31 present the results (these results were obtained with FreeFem++ v.4.5; FreeFem++ v.4.11 generates a slightly different mesh, whereby subtle differences might be observed). As for the effectivity indices $I_{\mathrm{eff},\ell}$ given by (15), for the equilibrated fluxes given by (10), they are greater or equal to one, rather close to one, but do not tend here to one, neither with the mesh refinement, nor with the polynomial degree increase. For Figure 30, where $p = p' = 1$, $I_{\mathrm{eff},\ell}$ takes the value 1.15228 (1.13601 for the mesh of FreeFem++ v.4.11), whereas for the same mesh with $p = p' = 2$ of Figure 31, $I_{\mathrm{eff},\ell} = 1.19244$ (1.20664 for the mesh of FreeFem++ v.4.11).

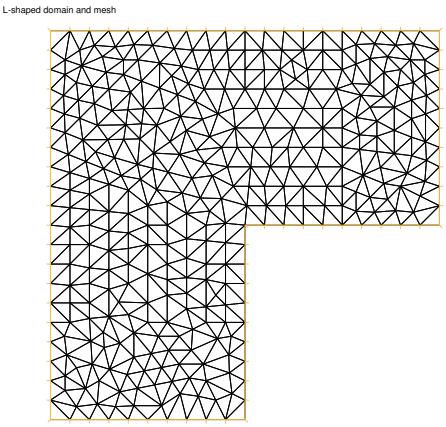

Figure 23: Domain Ω and the computational mesh $\mathcal{T}_\ell$ for the L-shaped example

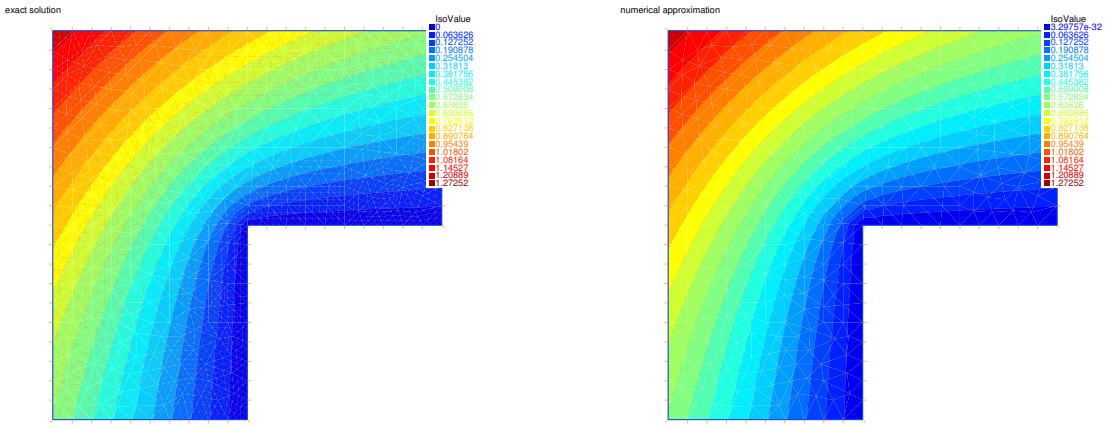

Figure 24: Exact solution u (left) and approximate solution u_ℓ (right, $p = 1$)

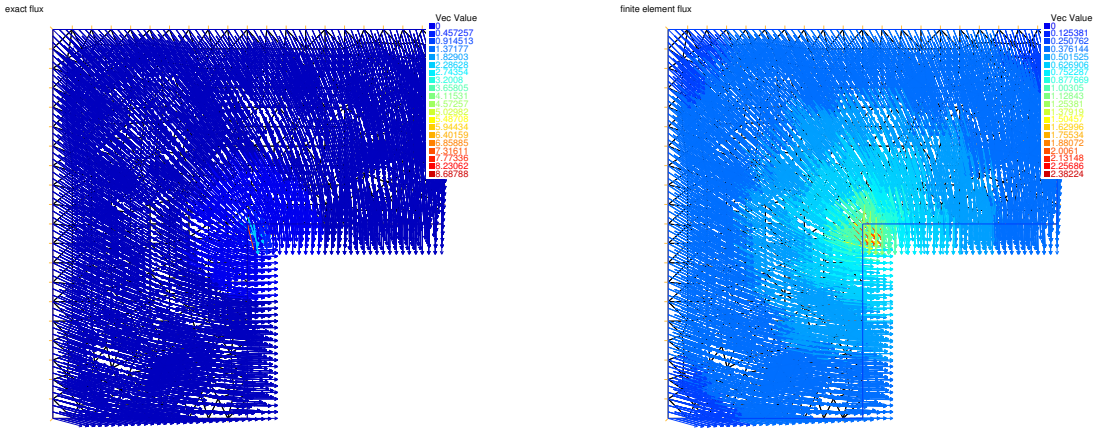

Figure 25: Flux of the exact solution $-\nabla u$ (left) and flux of the approximation $-\nabla u_\ell$ (right, $p = 1$)

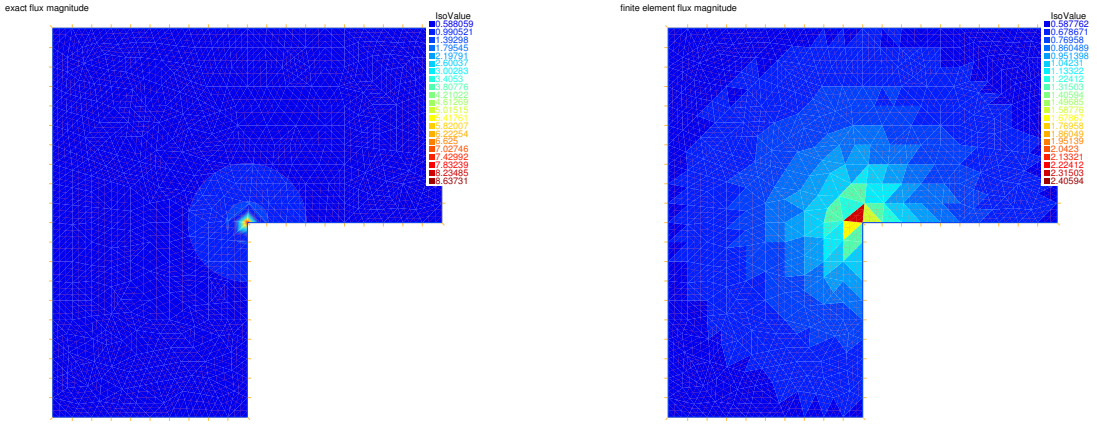

Figure 26: Magnitude of the fluxes, exact solution $|\nabla u|$ (left) and approximation $|\nabla u_\ell|$ (right, $p = 1$)

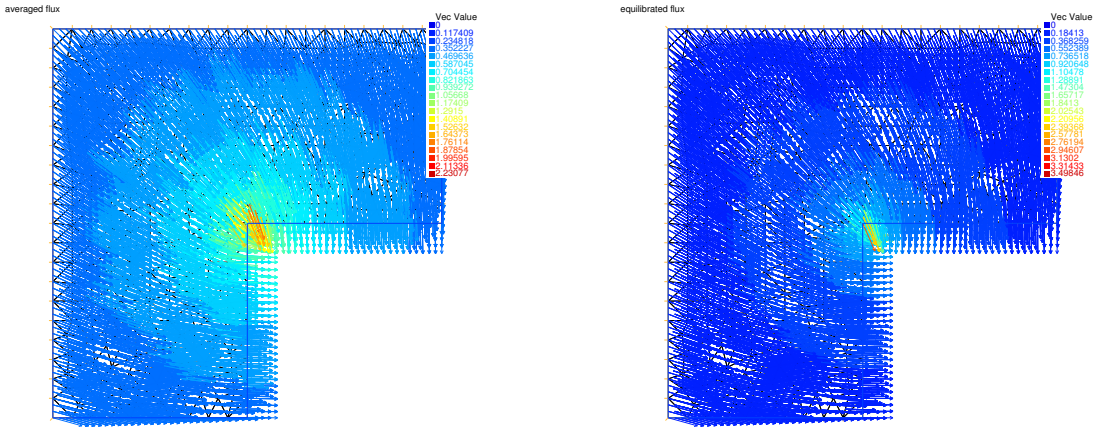

Figure 27: Averaged flux $\boldsymbol{\sigma}_\ell$ for $p = 1$ and $p' = 0$ (left) and equilibrated flux $\boldsymbol{\sigma}_\ell$ for $p = 1$ and $p' = 1$ (right)

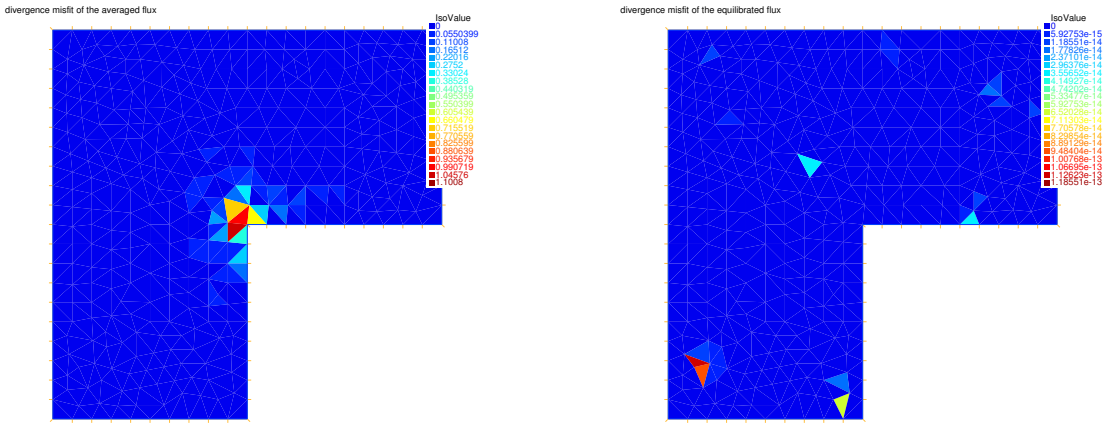

Figure 28: Divergence misfit of the averaged flux $\boldsymbol{\sigma}_\ell$ for $p = 1$ and $p' = 0$ (left) and divergence misfit of the equilibrated flux $\boldsymbol{\sigma}_\ell$ for $p = 1$ and $p' = 1$ (right)

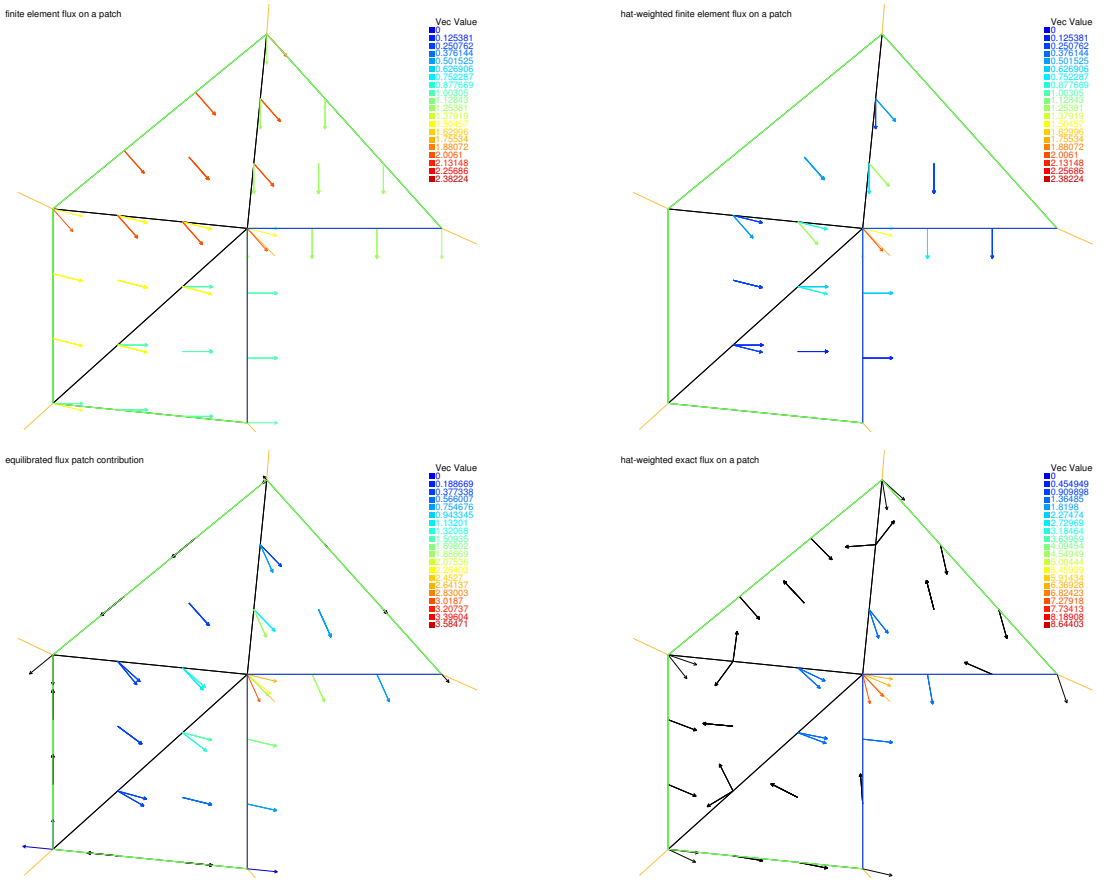

Figure 29: Finite element flux $-\nabla u_\ell$ (top left), the hat-function-weighted finite element flux $-\psi^{\boldsymbol{a}}\nabla u_\ell$ (top right), the equilibrated flux contribution $\boldsymbol{\sigma}_\ell^{\boldsymbol{a}}$ (bottom left), and the hat-function-weighted exact flux $-\psi^{\boldsymbol{a}}\nabla u$ (bottom right; there is some problem with FreeFem++ roundoff (the black arrows are (almost) zero) and rendering ($-\psi^{\boldsymbol{a}}\nabla u$ is indeed continuous)) on a patch subdomain $\omega_{\boldsymbol{a}}$ around the re-entrant corner vertex $\boldsymbol{a} = (0, 0)$, $p = 1$ and $p' = 1$

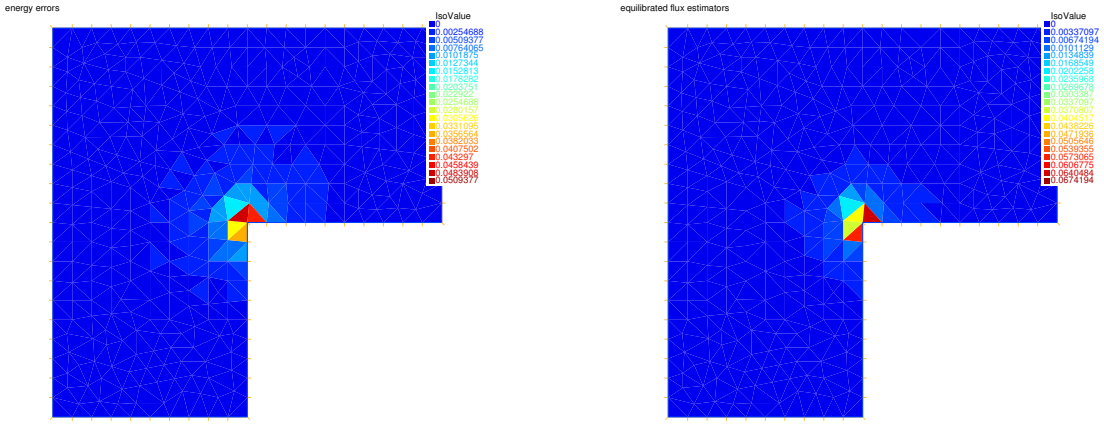

Figure 30: Elementwise errors $\|\nabla(u-u_\ell)\|_K$ (left) and estimators $\left[\|\nabla u_\ell+\boldsymbol{\sigma}_\ell\|_K+\frac{h_K}{\pi}\|f-\Pi_{p'}f\|_K\right]$ (right), equilibrated fluxes, $p=1$ and $p'=1$

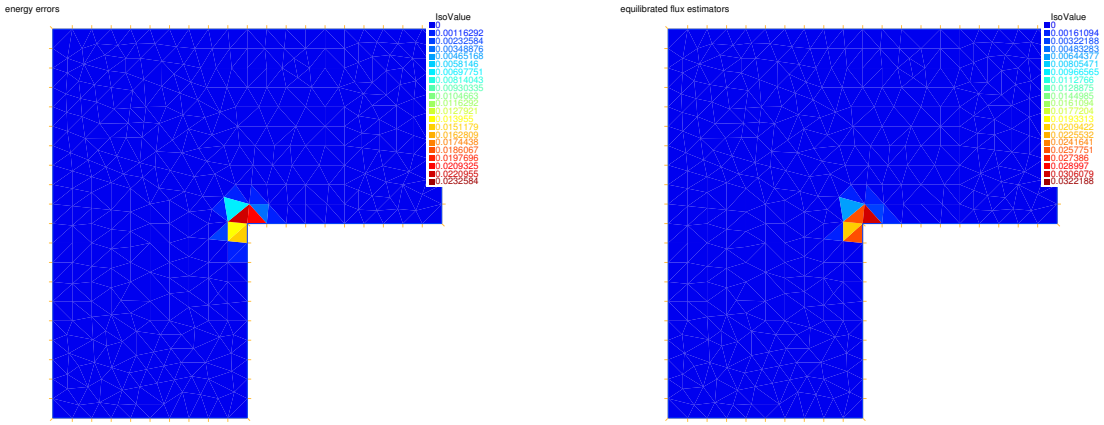

Figure 31: Elementwise errors $\|\nabla(u-u_\ell)\|_K$ (left) and estimators $\left[\|\nabla u_\ell+\boldsymbol{\sigma}_\ell\|_K+\frac{h_K}{\pi}\|f-\Pi_{p'}f\|_K\right]$ (right), equilibrated fluxes, $p=2$ and $p'=2$